Nanoscale Advances

ROYAL SOCIETY OF CHEMISTRY

PAPER

View Article Online
View Journal | View Issue

Cite this: *Nanoscale Adv.*, 2026, **8**, 123

Influence of temperature and pressure on preparing Ga nanowire arrays by press-based nanoinfiltration

Alberto A. Mendonça, * Leonardo Tomiatti, Kleber R. Pirota and Fanny Béron *

Nanoscale advanced materials are crucial for technological innovations. Among them, nanowires stand out due to their promising confinement effects and anisotropic properties derived from their elongated structure. However, this class of nanomaterials remains relatively underexploited, primarily due to fabrication challenges. In this work, we implement an alternative method for preparing nanowire arrays by pressing liquid metal into nanoporous alumina templates with cylindrical pores. Gallium was used as the liquid metal due to its melting point near room temperature. An investigation exploring the impact of temperature and pressure on the infiltration factor and length of nanowires was performed, revealing some counterintuitive behaviors. Higher filling factors and longer nanowires were obtained at lower infiltration temperatures, closer to the solidification point, with better performance observed at intermediate infiltration pressures rather than at higher pressures. Under optimal conditions, over 10 million parallel Ga nanowires per square millimeter were produced, with an average diameter of 151 + 36 nm and a high aspect ratio of around 500.

Received 1st July 2025
Accepted 28th October 2025

DOI: 10.1039/d5na00640f

rsc.li/nanoscale-advances

1. Introduction

Among nanostructures, nanowires are particularly interesting due to their unidimensional geometry. Their high length-to-width and surface-to-volume ratios enhance properties such as anisotropy and sensitivity in chemical and biological aspects.[1] In addition, nanoscale confinement enables the exploration of significant changes in quantum conditions, including modifications in energy level configurations.[2] As a result, properties such as magnetism and thermal, electrical, or optical conductivity can differ significantly between the axial and transverse directions. These unidimensional nanoscale characteristics have been extensively studied for various applications.[1–3]

Over the past two decades, semiconductor nanowires with lengths reaching millimeters and diameters limited to hundreds of nanometers have been studied due to the different conducting properties expected for one-dimensional materials.[3] Researchers have developed numerous axial and radial nanowire heterostructures, exploring their distinct electronic and photonic properties.[4–7] Moreover, nanowires may differ in phonon transport properties compared to their bulk counterparts. For example, silicon nanowires with rough surfaces and approximately 50 nm in diameter demonstrated a 100-fold decrease in thermal conductivity.[8] This resulted in a figure of merit of about 0.6 at room temperature – a considerable value for thermoelectric applications. Furthermore, the first fully integrated nanowire-based system for direct solar water splitting was developed in 2013.[9] A few years later, the same research group created a hybrid system combining semiconducting nanowires with *S. ovata* bacteria, where the nanowires capture sunlight while the bacteria facilitate the conversion of carbon dioxide and water in a synthetic photosynthesis process.[10] Beyond thermoelectrics and solar energy conversion and storage, nanowires have also played a significant role in advancing battery materials, piezoelectric technologies, and medical applications, as non-invasive drug delivery.[1,11]

However, the preparation of nanosized elongated materials with compositional tunability and high homogeneity remains challenging. A well-established preparation method for synthesizing metallic, metal oxide, and semiconductors nanowires with high purity and efficient growth control is the Vapor–Liquid–Solid (VLS) procedure.[1,12,13] In this method, liquid alloy droplets containing a metal catalyst are formed at high temperature by adsorbing vapor-phase components. Once the alloy becomes supersaturated, its composition exceeds the equilibrium concentration, and precipitation occurs at the liquid–solid interface. Continuous supply of vapor species sustains the one-dimensional (1D) nanowire growth. Although highly versatile and typically requiring only minutes to hours for sample preparation, this method has some drawbacks, including the need for avoiding catalyst contamination, the high temperature requirement, and the influence of catalyst

Instituto de Física Gleb Wataghin, Universidade Estadual de Campinas, 13083-859 Campinas, SP, Brazil. E-mail: betophys@ifi.unicamp.br; fberon@ifi.unicamp.br

size on nanowire diameter. Consequently, achieving uniform diameters can be challenging.

The Solution–Liquid–Solid (SLS) method is a variant of VLS growth that is conducted in solution, or in solvent dispersion.[14,15] In this approach, the precursor decomposes or reacts in solution, releasing atoms that dissolve into the liquid catalyst particle. When the catalyst becomes supersaturated, a solid nanowire nucleates and grows from it, analogous to the VLS mechanism, but with precursors supplied from the solution rather than the vapor phase. As in VLS, the catalyst governs the growth dynamics, enabling high crystal quality and purity. This method has been applied mainly for growing colloidal semiconductor nanorods and nanowires.[14] This method is usually less versatile in terms of the variety of materials it can prepare and more time-consuming, and has greater difficulty in forming long nanowires. On the other hand, it is performed at lower temperatures, typically between 200 °C and 350 °C, compared to around 1000 °C for VLS. Because of this and other factors, SLS is generally more economical.

Another established method is Chemical Vapor Deposition (CVD), a versatile and efficient method for synthesizing metallic, oxide, and especially Si-based semiconductor nanowires.[1,16,17] Here, preparation time also varies from minutes to hours, thus making it a relatively rapid process. While it offers excellent control over nanowire quality and deposition parameters, it remains challenging due to its high temperature requirements, high costs, complicated processes, and low yield.

On the other hand, template-assisted methods are versatile and low-cost, utilizing nanoporous templates to guide the growth of nanowires, such as Anodized Aluminum Oxide (AAO), as shown in Fig. 1.[1,18–20] These templates exhibit a high density of parallel nanopores, periodic spatial arrangement, and tunable shapes, allowing for various specific geometries.[20] In addition, once the template membrane is removed, free-standing nanowires can be obtained. Some distinct procedures are employed to grow nanowires using these templates; among them, electrochemical deposition is arguably the most popular. This cost-effective and environmentally friendly technique is widely used to fabricate metallic and semiconductor nanowires and can also produce nanocomposite materials.[1,21,22] Unlike previous methods, nanowires in this approach are grown at approximately room temperature, with their formation primarily controlled by the template structure. However, this method presents some limitations: the resulting crystalline quality is low, as the samples are typically polycrystalline or even amorphous, and certain chemical elements are unsuitable for this technique.

A promising alternative to address the challenges of the electrodeposition is the Metallic Flux Nanonucleation (MFNN),[23] which enables the combination of a wide range of elements, much like its bulk counterpart, the metallic flux method.[24] This latter technique is traditionally used to grow bulk single crystals by slowly cooling a high-temperature melt, where elements with higher melting points dissolve into a bath of a lower-melting-point element. The MFNN approach is quite similar, but crystal nucleation and growth are guided by the nanopores, leading to the formation of high-quality crystalline

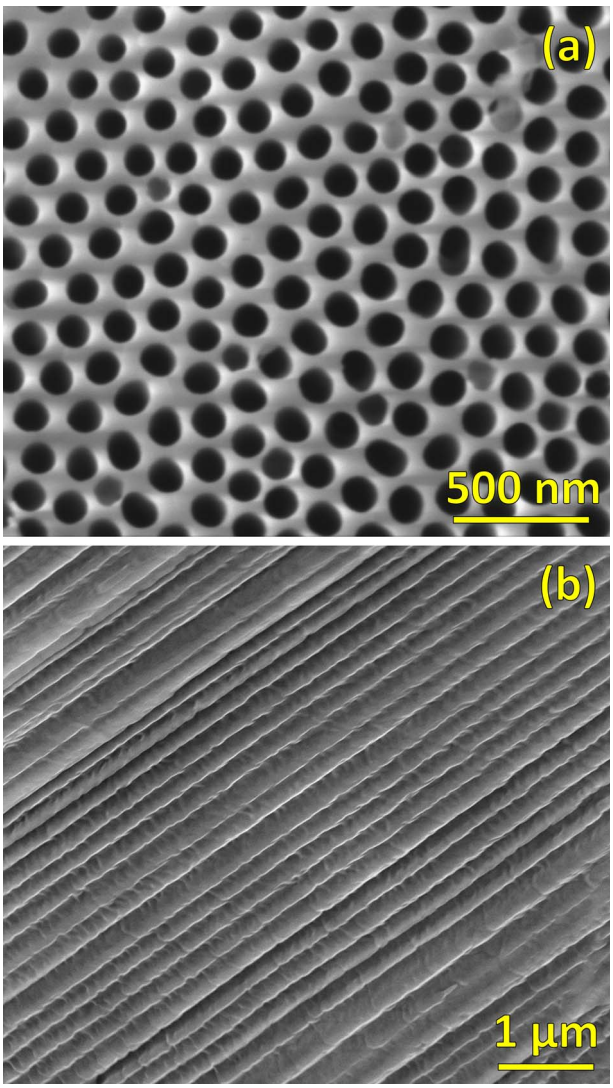

Fig. 1 Secondary electron Scanning Electron Microscopy (SEM) images showing a typical nanoporous AAO template: (a) surface with open nanopores and (b) cross-section of a broken membrane.

nanowires.[25] Although highly versatile and capable of producing single-crystal structures, this method requires elevated temperatures and is time-consuming, typically taking about a week to complete. In addition, due to the lack of an external force driving the elements into the nanopores, this technique may face difficulties in properly filling them, sometimes resulting in nanowires forming outside the templates.

Another template-based method is based on pressing liquid materials against nanoporous templates, here referred to as press-based nanoinfiltration (PBNI). Because AAO membranes exhibit enhanced mechanical strength under high pressure, they are particularly suitable for liquid infiltration driven by an applied load.[26,27] PBNI has been used for several decades and has proven capable of achieving high filling factors and long nanowires in procedures lasting less than 1 h. For example, C. A. Huber *et al.* reported an extensive study on electric field patterns over the surface of nanowires arrays for In, Sn, Al, Se,

Te, GaSb, and Bi_2Te_3, hydraulically pressed into AAO templates.[28] Other similar studies infiltrating liquid materials into AAO templates are available in the literature, such as Bi nanowires with diameters as small as 13 nm and lengths of 30–50 μm injected using high-pressure argon gas,[29,30] or with diameters reaching 15 nm and lengths around 10 μm infiltrated through a hydraulic jack.[31] Furthermore, single-crystalline nanowires with diameter ranging from 15 to 300 nm and length around 10 μm were obtained by hydraulically pressing molten Sn into AAO templates.[32,33] Finally, In-based nanowires with diameters of approximately 330 nm and lengths around 10 μm were prepared by hydraulic pressing for studying electroluminescence devices,[34] and nanowires with diameters around 350 nm and lengths of almost 50 μm were fabricated by mechanical pressure for thermometer applications.[35]

Certainly, PBNI is a practical, scalable, and highly cost-effective approach for fabricating nanowires from low-melting-point materials. It is appropriate for applications where production cost and volume are more critical than crystalline quality. However, it is not suitable for high-melting-point materials and presents challenges in controlling crystallinity due to the rapid formation of nanowires and potential pressure gradients along their length, which may lead to the formation of different phases and even phase segregation. A promising alternative is pressing materials into the nanopores of the AAO template using PBNI so that these filled nanopores can be used in the MFNN process, which serves to mix the elements at high temperatures and produce single-crystalline nanowires through slow cooling. This approach may overcome the previously mentioned issue of MFNN facing difficulties with nanopore infiltration. It is also important to highlight that the penetration and solidification of nanowires under pressure in the PBNI process can play a decisive role in stabilizing phases that would not be achievable using other methods where pressure is absent. A comparative summary of the nanowire preparation methods discussed above is presented in Table 1.

As noted above, the literature on the PBNI method has largely explored the preparation of nanowire arrays with a single element or, in a few cases, very specific binary alloys such as GaSb and Bi_2Te_3.[28] One metal that has surprisingly not been explored by this method is Ga, a well-known element for transforming into a liquid metal around room temperature. Bulk Ga usually solidifies in the orthorhombic α-phase, but others structures can be obtained, due to the presence of several metastable phases.[36] These different metastable structures are related to the sample preparation method, usually associated with pressure[37] or micro- and nanoconfinement while the material solidifies.[38–43] The most studied metastable phase of gallium is β-Ga, which can be obtained in bulk form but becomes more stable in undercooled micro- and nanoscale Ga specimens. This particular structure, along with other metastable phases, has been reported to remain stable in Ga droplets and nanowires fabricated using AAO templates prepared by different methods, where superconductivity was observed at temperatures at least 6 K higher than in bulk Ga.[38,40,41] Since Ga exhibits many metastable phases and low wettability,[44] it may be challenging to prepare nanowire arrays by PBNI. However, its melting point close to 30 °C makes it ideal for preparation using this method, requiring easy temperature control to become liquid.

Moreover, reports on liquid Ga under high pressure, combining synchrotron X-ray microtomography and energy dispersive X-ray diffraction, suggest the occurrence of a liquid–liquid transition associated with anomalous compressibility of the melt around 57 °C and 2.44 GPa.[45] Although no detectable liquid–liquid transition was observed under pressure up to 1.9 GPa at room temperature using *in situ* high energy X-ray pair distribution function and microtomography measurements, reverse Monte Carlo simulations revealed local structural features more closely related to those of solid Ga-II and Ga-III phases.[46]

To describe the liquid Ga infiltration phenomenon, the minimum pressure required for infiltrating liquids into nanopores of diameter D is commonly estimated using the so-called modified Washburn equation:[28,30,47]

$$P = \frac{-4\gamma\cos(\theta)}{D} \quad (1)$$

where γ is the surface tension of the liquid and θ is the contact angle between the liquid and the solid insulator. Eqn (1) shows that a minimum pressure is required for the liquid to enter the nanopore in the case of a non-wetting liquid, where $\theta > 90°$, since capillary forces do not drive infiltration. Furthermore, the smaller the nanopore diameter or the higher the surface tension, the greater the pressure required for infiltration to occur.

Another approach quantifies the length of the liquid column penetrating confined regions as a function of time:[48]

Table 1 Comparison of various nanowire synthesis methods in terms of sample quality and manufacturing considerations. The number of stars indicates the relative level of each characteristic associated with the preparation process

Method	Crystal quality	Scalability	Processing time	Temperature	Cost
CVD	★★★★★	★	★★	★★★★	★★★★
VLS	★★★★★	★★	★★	★★★★	★★★
SLS	★★★	★★★★	★★★	★★★	★★
AAO + El. Dep.	★★	★★★★★	★	★	★
AAO + NNFM	★★★★★	★★	★★★★★	★★★★	★★★
AAO + PBNI	★★★	★★★★★	★	Melting point	★

$$x = \left[\frac{R^2 t}{4\eta}\left(\Delta P + \frac{2D_f}{R}\right)\right]^{1/2} \quad (2)$$

where x is the distance reached by the liquid into the nanopore, R is the radius of the nanopore, t is the time, η is the viscosity, ΔP is the applied pressure, and D_f is the driving force. This driving force is associated with the surface tension and contact angle by the expression $D_f = \gamma_{sv} - \gamma_{sl} = \gamma_{lv} \cdot \cos(\theta)$, where γ_{sv}, γ_{sl}, and γ_{lv} are solid–vapor, solid–liquid, and liquid–vapor interfacial tension, respectively.[49,50] Therefore, both the applied pressure and the temperature, which modify the viscosity and the driving force, are expected to play an important role in the penetration process. A simple estimation applying a pressure of 3 MPa against liquid Al to infiltrate nanopores with $R = 1$ μm shows penetration of around 1 cm in 0.4 seg, a high filling rate.[49] Moreover, an experimental demonstration of rapid nanowire formation using the PBNI method was provided by C-C. Chen *et al.*, who prepared Sn nanowires – 60 nm in diameter and 10 μm in length – in nanoporous AAO templates using hydraulic pressing for less than 1 min.[33]

While preparing the first samples of Ga nanowire arrays *via* PBNI, we confirmed that temperature and pressure are critical parameters for the efficiency of nanowire formation, influencing both the nanopore filling factor and the nanowire length. However, these aspects have not been systematically evaluated in the literature, since the materials were melted at a temperature just above their melting point and then pressed without understanding the influence of these parameters. Therefore, in this work, we combine the fact that Ga has a melting point that is easily controllable with the need to understand how temperature and pressure influence nanowire formation *via* PBNI, in order to investigate the infiltration of a liquid metal into nanoporous AAO templates by fine tuning these parameters. Samples of Ga nanowire arrays at temperature ranging from 35 °C to 55 °C and with applied weight between 0.3 tons and 1.2 tons were prepared to evaluate the nanopore filling factor and nanowire length. We found that the models in eqn (1) and (2) were unable to describe many of our experimental results, indicating a strong and counterintuitive influence of temperature and pressure on the formation of nanowires.

Conversely, temperatures closer to the melting point of Ga, combined with low to intermediate applied loads, produced penetration behavior consistent with the pressure dependence predicted by eqn (2), yielding samples with a high filling factor and long nanowires. These results pave the way for the large-scale fabrication of parallel Ga nanowires whose properties may differ substantially from those of their bulk counterparts, opening avenues for diverse technological applications. For instance, Ga nanowires prepared by the NNFM method exhibited enhanced superconductivity compared to bulk Ga, attributed to the stabilization of an alternative phase under confinement.[41] Potential applications include superconductors, photon or molecular sensors, and superconducting microwave resonators enabled by the high density of the nanowire array.[51–53] Ga nanostructures also hold promise for optical and plasmonic devices, as liquid Ga offers tunable optical responses from the ultraviolet to the near-infrared through external stimuli such as applied load.[54,55] Additional emerging applications involve flow-focusing microfluidic systems for nanomaterial synthesis, soft metallic conductors or self-healing circuits derived from the liquid nature of Ga, and energy-harvesting devices based on electrowetting phenomena.[56]

2. Materials and methods

2.1. Nanoporous aluminum oxide template

A nanoporous alumina template was synthetized by hard anodization of electropolished aluminum disks with 99.999% purity, 25 mm diameter and 0.5 mm thickness. Initially, to release internal stresses, the aluminum disk was annealed in a tubular furnace under nitrogen gas flow with a heating rate of 15 °C min^{-1} up to 400 °C, where the temperature was held for 3 h. The electropolishing step used a 1 : 3 volumetric solution of perchloric acid and ethanol at around −10 °C with a limiting current of 3 A for 2 min. Then, an anodization process was carried out to grow a nanoporous alumina membrane on the Al disk, exhibiting a structure of close-packed hexagonal cells.[19] Highly ordered nanopores with diameters ranging from 20 nm to 200 nm can be obtained depending on the electrochemical conditions used. Smaller pore diameters are typically achieved through mild anodization, whereas the hard anodization mode produces larger pores.[57] Post-processing steps can further tune the nanopore diameter by chemical etching.[19]

Here, the anodization process was carried out at 0.5 °C with a solution of oxalic acid dihydrate and deionized water, with a concentration of 37.8 g L^{-1}, and platinum as the counter-electrode. The electrochemical procedure started by applying 40 V for 3 min, a mild anodization step, before raising the voltage at a 0.8 V s^{-1} rate until reaching 120 V, which was maintained for 2 h for a hard anodization step.[19,57] The resulting nanoporous AAO template presents 30% porosity, nanochannels of 80 μm length and an average diameter of 151 ± 36 nm, whose distribution is shown in Fig. 2. After anodization,

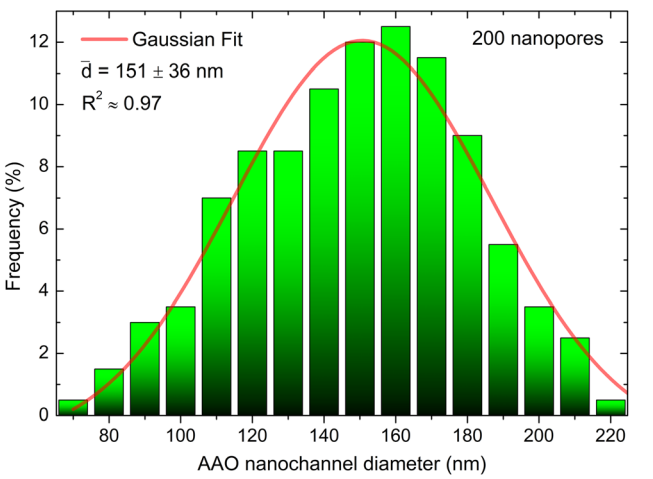

Fig. 2 Nanopore diameter distribution of the prepared AAO template with its respective Gaussian fit. The analysis was performed using 200 nanopores at the top of the surface.

the remaining aluminum was removed by chemical etching performed with a copper solution composed of Cu(II) chloride dihydrate, hydrochloric acid, and deionized water in a proportion of 34 g : 1 L : 1 L, respectively. Since an oxide barrier remains at the nanopore bottom, only one extremity of the nanopores is open. Finally, the alumina template was crystallized using a muffle furnace at a heating rate of 0.6 °C min^{-1} up to 900 °C for 2 h, followed by cooling down to room temperature after turning off the furnace.

2.2. Press-based nanoinfiltration (PBNI)

Arrays of nanowires were prepared by pressing a AAO template fragment of around 2 × 2 mm^2 against pure Ga using a hydraulic press. For standardization purposes, Ga was prepared in a thick plane shape, produced by melting a mass of 0.15 g of 99.99% purity to form a drop, which was subsequently solidified and then pressed under 0.5 ton.

The setup for the Press-Based Nano Infiltration (PBNI) procedure is shown in Fig. 3. First, a climate-controlled environment was established to prevent Ga from melting. One key point is that we positioned the standardized Ga disk below the AAO template, with its nanopores facing downwards. As the pressure cell was closed, the piston was mechanically fixed to prevent movement during the vacuum pumping stage. This avoided premature pressing caused by atmospheric pressure, ensuring that the piston only made contact with the Ga once the target temperature was reached. Using a mechanical pump, a vacuum of approximately 6 × 10^{-3} torr was achieved in 20 min. Simultaneously, a resistive heater warmed the piston up to the target temperature. Upon releasing the piston, the press force was increased to the chosen value and maintained for 30 min. We observed that fine-tuning the applied weight may be required due to system thermalization, especially during the initial pressing period. Thereafter, the heater was turned off, allowing the system to cool down freely for 1 h, reaching a temperature below the Ga melting point, while the applied weight was maintained. Finally, the sample, surrounded by solid Ga, was removed upon opening the pressure cell.

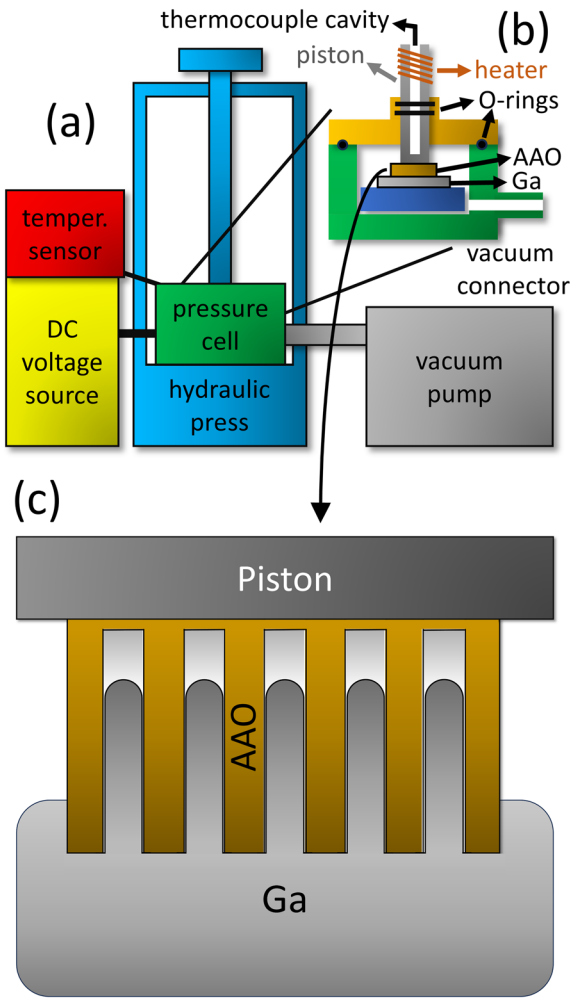

Fig. 3 Schematic of (a) press-based nano infiltration system, (b) pressure cell, and (c) an expanded view of the AAO surroundings.

Throughout this work, the applied load from the hydraulic press, measured in tons, was converted to pressure (Pa) for use in some graph axes. The pressure was estimated using $P = mg/A$, where $g = 9.8$ m s^{-2} is the acceleration due to gravity, and A is the effective contact area, calculated as the total sample area (≈ 4 mm^2) minus the area occupied by the nanopores. Considering a porosity of 30%, the resulting effective area was approximately 2.8 mm^2. Edge effects associated with sample borders or nanopore openings were neglected.

Although friction between the piston and the O-ring – lubricated with vacuum grease – may introduce slight resistance to motion, it was observed that the piston descended spontaneously during chamber evacuation, driven solely by external atmospheric pressure. Therefore, for the purpose of estimating the applied pressure, frictional effects were considered negligible.

In this work, twelve samples were prepared by pressing molten Ga on different fragments of the same AAO template, under applied weights of 0.3, 0.6, 0.9, and 1.2 tons at temperatures of 35 °C, 45 °C, and 55 °C. For testing reproducibility, five additional samples were pressed under 0.6 tons at 35 °C.

2.3. Ga infiltration analysis

We characterized the material infiltration results using two parameters: the pore filling factor (the proportion of infiltrated pores) and the penetration length of Ga along the nanopores of the template. Since we did not observe partially filled pores (see Fig. 4(a)), this parameter was not considered in the conducted analysis.

The samples were analyzed by Scanning Electron Microscopy (SEM) imaging using both Thermo Fisher Scientific Quanta 650 FEG and 250 FEG microscopes, with the beam voltage set to 20 kV. To enhance the contrast between the infiltrated Ga and the AAO template, we used the backscattered electron mode, without conductive coating, since the atomic number (Z) of Ga ($Z = 31$) is much higher than that of Al and O ($Z = 13$, and $Z = 8$, respectively). The arrays were imaged in two configurations: a surface view of the AAO with initially open pores, to calculate

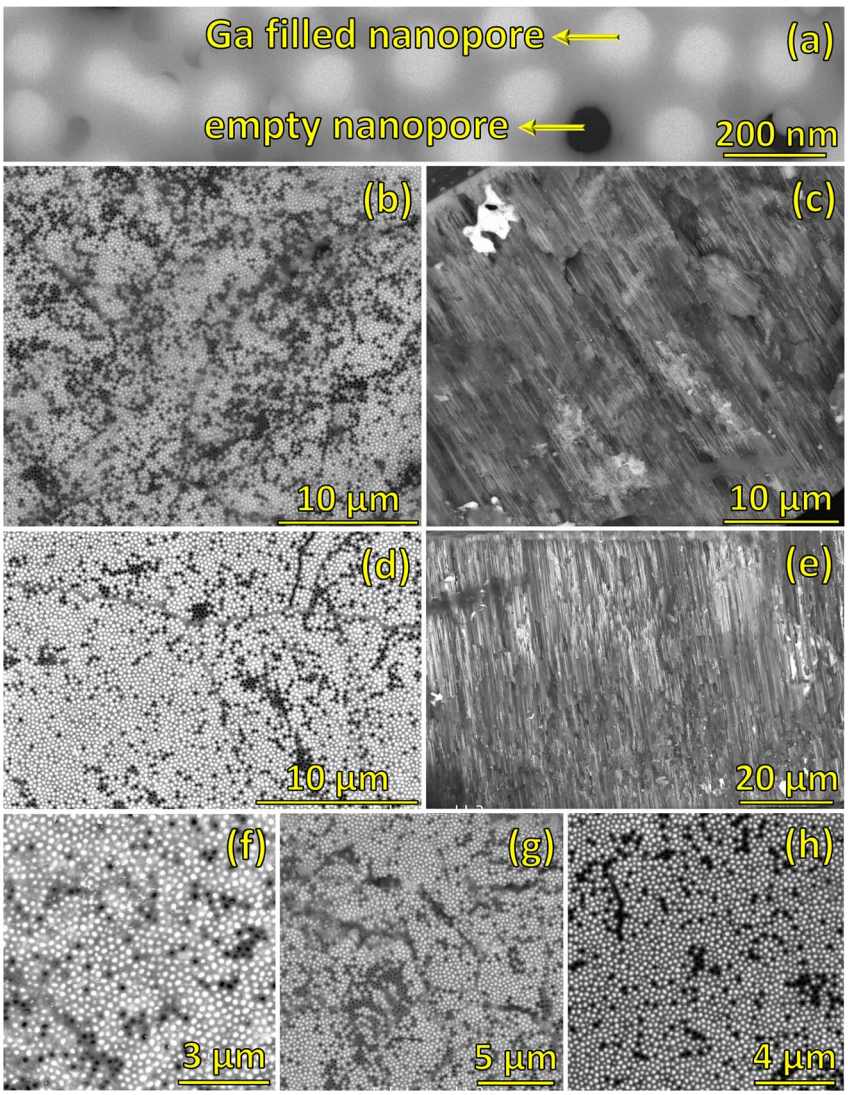

Fig. 4 Backscattered electron SEM images showing Ga nanowires infiltrated at 35 °C and under 0.6 tons. Surface morphology of the template at (a) high and (b) intermediate magnifications, and (c) cross-section of a fractured template. Panels d–h show four additional samples prepared independently under the same conditions, used to assess reproducibility.

the pore filling factor, and a cross-sectional view, to estimate the Ga infiltration length.

The analysis of the Ga filling factor within the nanopores was conducted using a Python script.[58] Based on the local contrast in the backscattered electron SEM images, the empty pores, filled pores, and alumina regions of the AAO template surface were identified. The filling factor was calculated as the ratio between the area of the filled nanopores and the total nanopores area, *i.e.*, both empty and filled.

Since determining the length of the obtained nanowires is challenging due to the irregular template fracture – and considering that a certain portion of the nanowires remains attached to the complementary piece of the broken template – a semi-quantitative method was employed to classify the infiltration lengths. Samples in which the nanowires typically measured less than 30 μm were considered short, those with lengths between 30 and 60 μm were identified as intermediate, and those exceeding 60 μm (on a total template thickness of 80 μm) were categorized as long.

3. Results and discussion

3.1 Morphology and reproducibility

Parallel Ga nanowires were prepared by the PBNI method to study pressure-induced Ga infiltration in nanoporous alumina templates with cylindrical nanopores approximately 151 ± 36 nm in diameter and 80 μm in length. SEM images of a sample obtained at 35 °C and under 0.6 tons are seen in Fig. 4(a)–(c). Portions with Ga appear brighter while the AAO template and empty nanopores range from gray to dark, as highlighted in Fig. 4(a). Examination of the surface with open pores – where infiltration occurred – reveals no evidence of partially filled nanopores.

Under these pressing conditions, we observed a high filling factor of around 75% for this sample, as shown in Fig. 4(b), with long nanowires completely crossing the template, as shown in panel (c). Taking into account its filling factor and the number of nanopores per area, this sample presents around 10 million nanowires per square millimeter. To evaluate fabrication reproducibility, five additional samples were prepared under the same conditions, 35 °C and 0.6 tons, four of which are shown in Fig. 4(d)–(h). The results show an average filling factor value of 80% with a standard deviation of around 8%. In all cases, the liquid Ga penetrated the entire length of the nanopores, attesting to the considerable reproducibility of the nanowire array preparation method.

3.2 Filling factor

The filling factor results for each temperature and pressure combination were mapped onto a contour color plot to visually represent variations in response to parameter changes, as shown in Fig. 5(a). Both temperature and pressure play a crucial role in determining the proportion of infiltrated nanopores. Regarding temperature, the filling factor reaches its highest values as it approaches the melting point of Ga (~30 °C), as observed in the map and emphasized in the curves of Fig. 5(b). For the lowest applied weight of 0.3 tons, the filling factor increases with temperature. On the other hand, under higher applied weights the increase in temperature, especially above 50 °C, proved to be an impediment to achieving high filling factors.

To compare the experimental values of applied weight with the minimum pressure required for infiltration according to eqn (1) – and its temperature dependence as well – we used the surface tension of Ga with similar purity to our samples:[59]

$$\gamma = (715 \pm 1.0) - (0.090 \pm 0.002)(T - T_{\text{melting}}) \quad (3)$$

where $T_{\text{melting}} = 29.7646$ °C.[60] Between 35 °C and 55 °C, γ decreases by only 0.25%, indicating a minimal impact within this temperature range. Similarly, the contact angle θ is expected to remain nearly constant, as it depends solely on surface tension, according to Young's equation.[50,61] In our experiments, Ga was observed to form micro- and nanospheres on the alumina templates (not shown), indicating a high contact angle, which is consistent with literature reports for Ga droplets on glass surfaces.[44] It is known that templates with surface roughness result in a range of possible contact angles rather than a single well-defined value.[61] In this work, we estimate an average contact angle of $\theta = 160°$ for the following calculations, which is typical for Ga and similar low-wettability liquids.[33,44,62]

Using the definition of pressure as force per unit area, for the lowest applied weight of 0.3 tons, the resulting pressure is around 1.05 GPa. This value is approximately 59 times greater than the minimum pressure required to infiltrate Ga at 35 °C expected from the modified Washburn model of eqn (1), which is around 17.8 MPa. Once again, since γ varies little within the studied temperature range, the minimum infiltration pressure predicted by eqn (1) is not expected to approach the levels

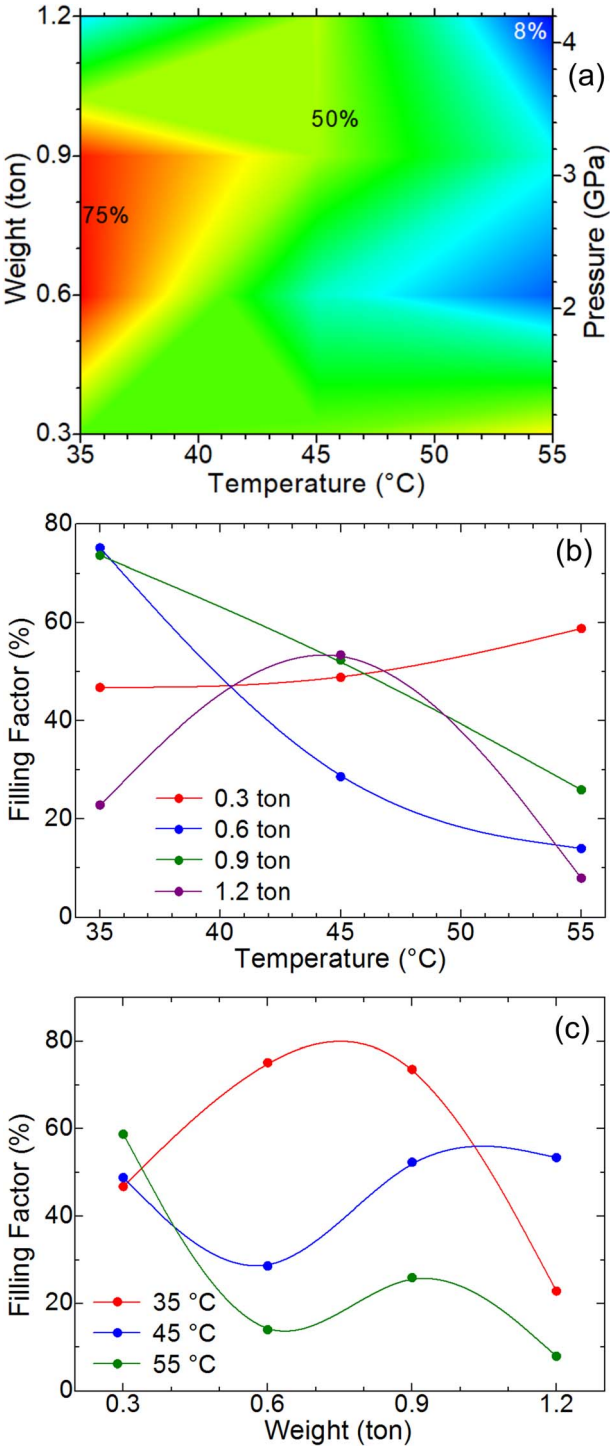

Fig. 5 The filling factor of Ga nanowires (a) exhibited as a color map as a function of temperature and weight applied by the hydraulic press, (b) as a function of temperature for each applied weight and (c) as a function of applied weight for each isothermal curve. The pressure axis values in (a) were estimated taking into account 30% porosity.

achieved during the hydraulic pressing process, as it remains nearly unchanged at 45 °C and 55 °C.

Furthermore, the resistance to liquid infiltration can be explained by the work of adhesion (W_a), which quantifies the

energy required to separate a liquid from a solid surface per unit area. According to the Young–Dupré equation:[63]

$$W_a = \gamma(1 + \cos(\theta)) \quad (4)$$

The calculated W_a is approximately 43.1 mJ m^{-2}, a relatively low value.[63,64] Variations in W_a are unlikely to significantly impact the filling factor within the studied temperature interval due to its dependence on γ and θ. Therefore, the pronounced temperature-induced changes in Ga infiltration observed in Fig. 5 cannot be fully explained by conventional infiltration models.

Additionally, the applied pressure on liquid Ga does not result in a monotonic increase in the filling factor, as shown in Fig. 5(c). At 35 °C, the infiltration dependence on pressure peaks at intermediate values before decreasing as the applied weight increases to 1.2 tons. No clear trend is observed at 45 °C and 55 °C, although at higher temperatures, the filling factor tends to decrease more noticeably with increasing pressure. Therefore, in terms of infiltration efficiency, the highest filling factor was achieved at 35 °C under 0.6 to 0.9 tons. These parameters are critical for achieving high-yield Ga nanowire fabrication by PBNI, with 0.6 tons being the optimal condition to prevent both mechanical damage to the AAO template and long-term denting of the steel components involved in pressing. Conversely, sample preparation at 55 °C and 1.2 tons produced the lowest filling factor, reaching only 8%, indicating that excessive temperature and pressure hinder the infiltration of liquid Ga into the nanopores of the AAO template.

3.3 Nanowire length

A color map representing short, intermediate, and long nanowires for the twelve samples was generated, as shown in Fig. 6(a). Once again, samples prepared at 35 °C with applied weights ranging from 0.6 to 0.9 tons stood out, indicating that this configuration is optimal not only for achieving a high filling factor but also for controlling nanowire length. The smallest lengths were identified not only at lower pressures, which is intuitive, but also at high pressure at 35 °C, a behavior similar to that observed in the filling factor data in Fig. 5.

While the Washburn equation is useful for describing the initial stage of the infiltration process, eqn (2) is more appropriate for modeling the subsequent penetration, since it accounts for the liquid viscosity.[65] For temperatures a few tens of degrees Celsius above the melting point of Ga, its viscosity is given by:[66]

$$\eta = 0.00217 - 7.1 \times 10^{-6}\,T \quad (5)$$

In the temperature range explored in this work, the Ga viscosity changes by approximately 7.3%, which is significantly greater than the 0.25% variation observed in surface tension. On the other hand, the driving force D_f is expected to remain nearly constant between 35 °C and 55 °C due to its dependence on γ and θ.[49,60] A region of the map exhibits an increase in depth x as ΔP rises, in agreement with eqn (2), as highlighted in Fig. 6(b). This region corresponds to temperatures near the melting point of Ga and low-to-intermediate applied pressures in our experiments, where the penetration color map from the model of eqn (2) was calculated, as presented in Fig. 6(c).

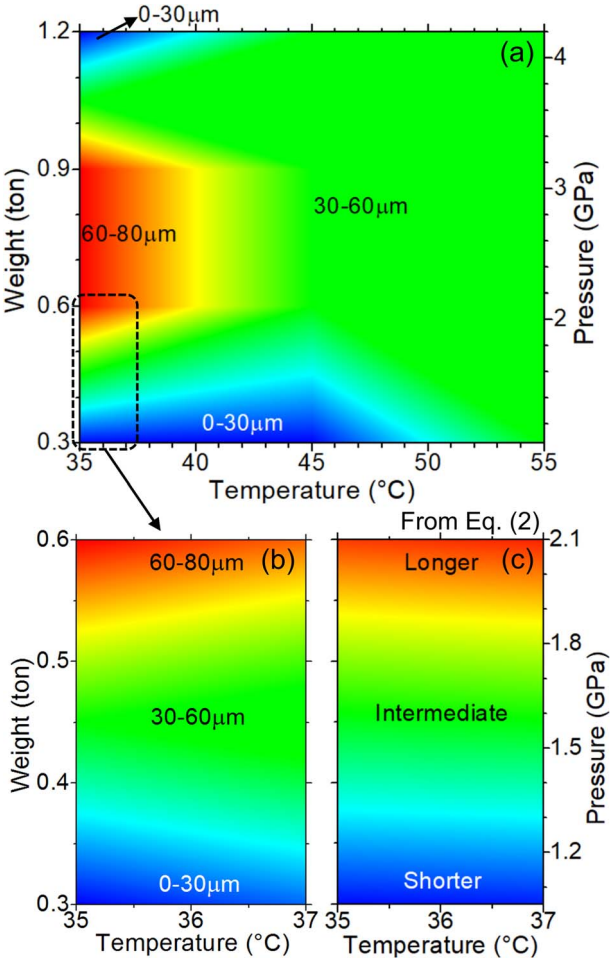

Fig. 6 (a) Color map of the typical Ga nanowire length as a function of temperature and applied weight. Expanded areas of (b) experimental and (c) eqn (2) results with t = 30 min. The pressure axis values were estimated taking into account 30% porosity.

The similarities observed between Fig. 6(b) and (c) within a limited range of temperature and pressure suggest that, as both parameters increase, additional factors beyond those considered in the models explored here begin to play a significant role in the infiltration process. Although the literature lacks data on pressure-dependent variations of surface tension and viscosity for liquid Ga, it is generally known that, for most liquids, surface tension tends to decrease[67,68] and viscosity tends to increase under pressure.[69,70]

These general trends of surface tension and viscosity for liquid metals and additional investigations with liquid Ga open new avenues for future experiments and simulations aiming to investigate the infiltration behavior of liquid Ga – and potentially other liquid metals – under more comprehensive conditions. To the best of our knowledge, the observations presented here have not been systematically reported in previous studies, which typically focus on estimating the minimum infiltration

pressure using the Washburn equation, followed by heating the system to the melting point and applying a load exceeding the calculated threshold.[28,30–33]

Further investigations will be conducted for modelling the sample preparation system and the liquid Ga infiltration phenomenon in the PBNI method, to achieve a more complete understanding of the behaviors of the filling factor and the nanowire length presented here. However, we emphasize that this work addresses two significant gaps:

(1) The establishment of optimal parameters for the reproducible fabrication of Ga nanowires with a high filling factor – reaching up to 80% – and a high aspect ratio exceeding 500. Such a high filling factor, combined with aligned and closely packed nanowires due to the template, enables the investigation of collective phenomena. For example, type-II superconductivity has already been reported for the β-Ga phase in nanowires.[41] With a high filling factor, the vortex structures that carry magnetic field lines may interact with neighboring superconducting nanowires. Furthermore, the high aspect ratio enhances anisotropy effects. Again, using type-II superconductivity as an example, it leads to the formation of vortices that may exhibit distinct structures depending on their orientation, either parallel or perpendicular to the nanowire length.[41] Finally, although confinement effects on Ga nanowires have been previously explored in the literature,[41] the samples prepared *via* PBNI are solidified under pressure, which may favor the stabilization of other metastable phases.[36–39] A complementary study on the structural phases observed in these Ga nanowires will be further reported. All these factors, combined with the advantages of a highly scalable, low-cost, and time-efficient method, position PBNI as a powerful approach for the rapid synthesis of nanowire-based systems.

(2) Although the PBNI method is not entirely new, a systematic investigation of the effects of pressure and temperature on nanowire formation had not been previously reported. The findings presented in this work emphasize the need for further studies to understand the infiltration behavior of liquid Ga, and potentially other liquid metals, into nanoporous alumina, a material widely used as a template for nanomaterial fabrication.[19,20] Liquid Ga infiltrating at temperatures closer to its melting point and under low to intermediate pressures showed better agreement with theoretical expectations compared to those formed at higher temperatures and pressures. These insights may spark further interest in exploring the limits of existing nanoinfiltration theories and emergent phenomena governing the dynamics of liquid nanomaterials under pressure in porous media.

4. Conclusions

Twelve samples of nanowire arrays were prepared using a hydraulic press to infiltrate liquid Ga into nanoporous alumina templates with around 4 mm^2. The nanopores present a diameter of 151 ± 36 nm and a length of 80 μm. The effects of temperature and pressure on the infiltration process were evaluated at temperatures of 35 °C, 45 °C, and 55 °C, and under applied weights of 0.3, 0.6, 0.9, and 1.2 tons. The samples prepared at 35 °C under 0.6 and 0.9 tons exhibited the highest filling factors and nanowire lengths, achieving nearly 80% pore filling and nanowires spanning the entire 80 μm of template. While a complete explanation for the observed behavior was not achieved, the time-dependent liquid penetration model captured important pressure-driven trends of the experimental data, especially at temperatures near the melting point of Ga and under lower applied pressures. The successful preparation of Ga nanowires with a high filling factor and aspect ratio using a simple, fast and cost-effective method offers promising opportunities for exploring new nanostructured materials and stabilizing metastable phases through pressure and confinement. Finally, the PBNI method holds great potential to enhance the filling factor and improve reproducibility in nanowire arrays prepared *via* MFNN, especially considering that the latter employs low-melting-point mixtures with a significantly higher mass of flux compared to that of the other constituent elements.

Author contributions

A. A. Mendonça: conceptualization, methodology, investigation, formal analysis, writing – original draft preparation. L. Tomiatti: conceptualization, methodology, software, formal analysis, writing – review & editing. K. R. Pirota: supervision, conceptualization, resources, funding acquisition, writing – review & editing. F. Béron: supervision, conceptualization, resources, funding acquisition, writing – review & editing.

Conflicts of interest

There are no conflicts to declare.

Data availability

The code for analysis of the Ga filling factor within the nanopores can be found at **https://doi.org/10.5281/zenodo.14602027**. The version of the code employed for this study is version 1.

Acknowledgements

A. A. Mendonça is supported by a postdoctoral grant from Fundação de Amparo à Pesquisa do Estado de São Paulo (FAPESP), 2022/16839-9. L. Tomiatti was supported by an undergraduate grant from Conselho Nacional de Desenvolvimento Científico e Tecnológico (CNPq), 124316/2024-7. The research group is supported by FAPESP, projeto Temático 2017/10581-1, CNPq 312762/2021-6, 421070/2023-4 and 443930/2023-6, and the Institutos Nacionais de Ciência e Tecnologia (INCT) of Spintronics and Advanced Magnetic Nanostructures (INCT-SpinNanoMag), CNPq 406836/2022-1. This research used facilities of the Brazilian Nanotechnology National Laboratory (LNNano), part of the Brazilian Centre for Research in Energy and Materials (CNPEM). The Scanning Electron Microscopy & Dual Beam Laboratory staff is acknowledged for assistance during the experiments (#20233515). This research used

facilities of LIMicro-IQ - Microscopy Core Facility (RRID:SCR_024633) at the Universidade Estadual de Campinas.

References

1 J. J. Mim, M. Hasan, M. S. Chowdhury, J. Ghosh, M. Hosne Mobarak, F. Khanom and N. Hossain, A comprehensive review on the biomedical frontiers of nanowire applications, *Heliyon*, 2024, **10**, e29244, DOI: 10.1016/j.heliyon.2024.e29244.

2 C.-Yi Hsu, A. M. Rheima, Z. S. Abbas, M. U. Faryad, M. M. Kadhim, U. S. Altimari, A. H. Dawood, A. d. j. al-bayati, Z. T. Abed, R. S. Radhi, A. S. Jaber, S. K. Hachim, F. K. Ali, Z. H. Mahmoud, G. B. pour and E. Kianfar, Nanowires Properties and Applications: A Review Study, *S. Afr. J. Chem. Eng.*, 2023, **46**, 286, DOI: 10.1016/j.sajce.2023.08.006.

3 E. Garnett, L. Mai and P. Yang, Introduction: 1D Nanomaterials/Nanowires, *Chem. Rev.*, 2019, **119**, 8955, DOI: 10.1021/acs.chemrev.9b00423.

4 M. S. Gudiksen, L. J. Lauhon, J. Wang, D. C. Smith and C. M. Lieber, Growth of Nanowire Superlattice Structures for Nanoscale Photonics and Electronics, *Nature*, 2002, **415**, 617, DOI: 10.1038/415617a.

5 L. J. Lauhon, M. S. Gudiksen, C. L. Wang and C. M. Lieber, Epitaxial Core-Shell and Core-Multishell Nanowire Heterostructures, *Nature*, 2002, **420**, 57, DOI: 10.1038/nature01141.

6 Y. Y. Wu, R. Fan and P. D. Yang, Block-by-Block Growth of Single-Crystalline Si/SiGe Superlattice Nanowires, *Nano Lett.*, 2002, **2**, 83, DOI: 10.1021/nl0156888.

7 M. T. Bjork, B. J. Ohlsson, T. Sass, A. I. Persson, C. Thelander, M. H. Magnusson, K. Deppert, L. R. Wallenberg and L. Samuelson, One-Dimensional Steeplechase for Electrons Realized, *Nano Lett.*, 2002, **2**, 87, DOI: 10.1021/nl010099n.

8 A. I. Hochbaum, R. K. Chen, R. D. Delgado, W. J. Liang, E. C. Garnett, M. Najarian, A. Majumdar and P. D. Yang, Enhanced Thermoelectric Performance of Rough Silicon Nanowires, *Nature*, 2008, **451**, 163, DOI: 10.1038/nature06381.

9 C. Liu, J. Y. Tang, H. M. Chen, B. Liu and P. D. Yang, A Fully Integrated Nanosystem of Semiconductor Nanowires for Direct Solar Water Splitting, *Nano Lett.*, 2013, **13**, 2989, DOI: 10.1021/nl401615t.

10 C. Liu, J. J. Gallagher, K. K. Sakimoto, E. M. Nichols, C. J. Chang, M. C. Y. Chang and P. D. Yang, Nanowire-Bacteria Hybrids for Unassisted Solar Carbon Dioxide Fixation to Value-Added Chemicals, *Nano Lett.*, 2015, **15**, 3634, DOI: 10.1021/acs.nanolett.5b01254.

11 A. I. Hochbaum and P. D. Yang, Semiconductor Nanowires for Energy Conversion, *Chem. Rev.*, 2010, **110**, 527, DOI: 10.1021/cr900075v.

12 A. Mirzaei, M. H. Lee, K. K. Pawar, S. P. Bharath, T.-U. Kim, J.-Y. Kim, S. S. Kim and H. W. Kim, Metal Oxide Nanowires Grown by a Vapor–Liquid–Solid Growth Mechanism for Resistive Gas-Sensing Applications: An Overview, *Materials*, 2023, **16**, 6233, DOI: 10.3390/ma16186233.

13 J. M. Redwing, X. Miao and X. Li, Vapor-Liquid-Solid Growth of Semiconductor Nanowires, *Handbook of Crystal Growth*, 2nd edn, 2015, pp. 399, DOI: 10.1016/B978-0-444-63304-0.00009-3.

14 F. Wang, A. Dong and W. E. Buhro, Solution–Liquid–Solid Synthesis, Properties, and Applications of One-Dimensional Colloidal Semiconductor Nanorods and Nanowires, *Chem. Rev.*, 2016, **116**, 10888, DOI: 10.1021/acs.chemrev.5b00701.

15 S.-L. Jheng, J.-y. Chen and H.-Y. Tuan, Solution-liquid-solid growth of $CuInTe_2$ nanowires as lithium-ion battery anodes, *Mater. Des.*, 2018, **149**, 113, DOI: 10.1016/j.matdes.2018.03.059.

16 K. Choy, Chemical vapour deposition of coatings, *Prog. Mater. Sci.*, 2003, **48**, 57, DOI: 10.1016/s0079-6425(01)00009-3.

17 R. A. Puglisi, G. Mannino, S. Scalese, A. La Magna and V. Privitera, Silicon nanowires obtained by low temperature Plasma-Based chemical vapor deposition, *MRS Adv.*, 2012, **1408**, 139, DOI: 10.1557/opl.2012.718.

18 J. Liu, S. Liu, H. Zhou, C. Xie, Z. Huang, C. Fu and Y. Kuang, Preparation of self-ordered nanoporous anodic aluminum oxide membranes by combination of hard anodization and mild anodization, *Thin Solid Films*, 2014, **552**, 75, DOI: 10.1016/j.tsf.2013.12.023.

19 A. R-Clavijo, O. C-Calero and M. M-González, Revisiting anodic alumina templates: from fabrication to applications, *Nanoscale*, 2021, **13**, 2227, DOI: 10.1039/D0NR07582E.

20 R. Xu, Z. Zeng and Y. Lei, Well-defined nanostructuring with designable anodic aluminum oxide template, *Nat. Commun.*, 2022, **13**, 2435, DOI: 10.1038/s41467-022-30137-6.

21 V. M. Prida, V. Vega, J. García, L. Iglesias, B. Hernando and I. Minguez-Bacho, Electrochemical synthesis of magnetic nanowires with controlled geometry and magnetic anisotropy, Magnetic Nano- and Microwires, Design, Synthesis, Properties and Applications, *Woodhead Publ. Ser. Electron. Opt. Mater.*, 2015, **41**, 41, DOI: 10.1016/B978-0-08-100164-6.00002-3.

22 S. Ruiz-Gómez, C. Fernández-González and L. Perez, Electrodeposition as a Tool for Nanostructuring Magnetic Materials, *Micromachines*, 2022, **13**, 1223, DOI: 10.3390/mi13081223.

23 K. R. Pirota, K. O. Moura, A. S. E. da Cruz, R. B. Campanelli, P. J. G. Pagliuso, and F. Béron, Intermetallic nanowires fabricated by metallic flux nanonucleation method (MFNN), Magnetic Nano- and Microwires, *Design, Synthesis, Properties and Applications, Woodhead Publishing Series in Electronic and Optical Materials*, 2nd edn, 2020, vol. 61, DOI: 10.1016/B978-0-08-102832-2.00003-7.

24 P. C. Canfield and Z. Fisk, Growth of single crystals from metallic fluxes, *Philos. Mag. B*, 1992, **65**, 1123, DOI: 10.1080/13642819208215073.

25 A. S. E. Cruz, R. B Campanelli, M. V. P. dos Santos, F. Fabris, J. Bettini, P. G. Pagliuso and K. R Pirota, Manganese silicide nanowires via metallic flux nanonucleation: growth mechanism and temperature-dependent resistivity,

Nanotechnology, 2022, **33**, 475704, DOI: 10.1088/1361-6528/ac893c.

26 A. Ullah, A. K. Kasi, J. K. Kasi and M. Bokhari, Fabrication of mechanically stable AAO membrane with improved fluid permeation properties, *Microelec. Eng.*, 2018, **187**, 95, DOI: 10.1016/j.mee.2017.11.019.

27 A. Bankova, V. Videkov, B. Tzaneva and M. Mitov, Mechanical stability of heat-treated nanoporous anodic alumina subjected to repetitive mechanical deformation, IOP Conf. Series, *J. Phys.:Conf. Ser.*, 2018, **992**, 012055, DOI: 10.1088/1742-6596/992/1/012055.

28 C. A. Huber, T. E. Huber, M. Sadoqi, J. A. Lubin, S. Manalis and C. B. Prater, Nanowire Array Composites, *Science*, 1994, **263**, 800, DOI: 10.1126/science.263.5148.800.

29 Zhang, J. Y. Ying and M. S. Dresselhaus, Bismuth quantum-wire arrays fabricated by a vacuum meltingand pressure injection process, *J. Mater. Res.*, 1998, **13**, 7, DOI: 10.1557/JMR.1998.0243.

30 Z. Zhang, D. Gekhtman, M. S. Dresselhaus and J. Y. Ying, Processing and Characterization of Single-Crystalline Ultrafine Bismuth Nanowires, *Chem. Mater.*, 1999, **11**, 1659, DOI: 10.1021/cm9811545.

31 Y. Bisrat, Z. P. Luo, D. Davis and D. Lagoudas, Highly ordered uniform single-crystal Bi nanowires: fabrication andcharacterization, *Nanotechnology*, 2007, **18**, 395601, DOI: 10.1088/0957-4484/18/39/395601.

32 C.-C. Chen, C.-G. Kuo and C.-G. Chao, Template Assisted Fabrication of Tin Nanospheres by Thermal Expansion and Rapid Solidification Process, *Jpn. J. Appl. Phys.*, 2005, **44**, 1524, DOI: 10.1143/JJAP.44.1524.

33 C.-C. Chen, Y. Bisrat, Z. P. Luo, R. E. Schaak, C.-G. Chao and D. C. Lagoudas, Fabrication of single-crystal tin nanowires by hydraulic pressure injection, *Nanotechnology*, 2006, **17**, 367, DOI: 10.1088/0957-4484/17/2/004.

34 F. Chen and A. H. Kitai, Application of indium nanowires to donor– acceptor pair luminescence, *J. Lumin.*, 2008, **128**, 1856, DOI: 10.1016/j.jlumin.2008.05.010.

35 P. Peng, Z. Su, Z. Liu, Q. Yu and Z. C. J. Bao, Nanowire thermometers, *Nanoscale*, 2013, **5**, 9532, DOI: 10.1039/C3NR03086E.

36 R. D. Heyding, W. Keeney and S. L. Segel, Metastable phases in gallium dispersions, *J. Phys. Chem. Solids*, 1973, **34**, 133, DOI: 10.1016/0022-3697(73)90068-1.

37 L. Bosio, Crystal structures of Ga(ll) and Ga(lII), *J. Chem. Phys.*, 1978, **68**, 3, DOI: 10.1063/1.435841.

38 E. V. Charnaya, C. Tien, K. J. Lin, C. S. Wur and Yu. A. Kumzerov, Superconductivity of gallium in various confined geometries, *Phys. Rev. B:Condens. Matter Mater. Phys.*, 1998, **58**, 467, DOI: 10.1103/PhysRevB.58.467.

39 D. Teske and J. E. Drumheller, Phases of gallium nucleated by small particles, *J. Phys.: Condens. Matter*, 1999, **11**, 4935, DOI: 10.1088/0953-8984/11/25/312.

40 E. V. Charnaya, C. Tien, M. K. Lee and Y. A Kumzerov, Superconductivity and structure of gallium under nanoconfinement, *J. Phys.: Condens. Matter*, 2009, **21**, 455304, DOI: 10.1088/0953-8984/21/45/455304.

41 K. O. Moura, K. R. Pirota, F. Béron, C. B. R. Jesus, P. F. S. Rosa, D. Tobia, P. G. Pagliuso and O. F. de Lima, Superconducting Properties in Arrays of Nanostructured β-Gallium, *Sci, Rep.*, 2017, **7**, 15306, DOI: 10.1038/s41598-017-15738-2.

42 D. Campanini, Z. Diao and A. Rydh, Raising the superconducting Tc of gallium In situ characterization of the transformation of α-Ga into β-Ga, *Phys. Rev. B*, 2018, **97**, 184517, DOI: 10.1103/PhysRevB.97.184517.

43 J. Liu, L. Song, Z. He, S. Wang, W. Zhang, H. Yang, F. Li, S. Li, J. Wang, H. Xiao, D. Xu, Y. Liu, Y. Wu, J.-Q. Wang, X. Shui, Y.-C. Hu, J. Shang and R.-W. Li, Size Dependent Phase Transformation of Liquid Gallium, *Small*, 2023, 2305798, DOI: 10.1002/smll.202305798.

44 Q. Xu, N. Oudalov, Q. Guo, H. M. Jaeger and E. Brown, Effect of oxidation on the mechanical properties of liquid gallium and eutectic gallium-indium, *Phys. Fluids*, 2012, **24**, 063101, DOI: 10.1063/1.4724313.

45 R. Li, L. Li, T. Yu, L. Wang, J. Chen, Y. Wang, Z. Cai, J. Chen, M. L. Rivers and H. Liu, Study of liquid gallium as a function of pressure and temperature using synchrotron x-ray microtomography and x-ray diffraction, *Appl. Phys. Lett.*, 2014, **105**, 041906, DOI: 10.1063/1.4891572.

46 R. Li, L. Wang, L. Li, T. Yu, H. Zhao, K. W. Chapman, Y. Wang, M. L. Rivers, P. J. Chupas, Ho-k. Mao and H. Liu, Local structure of liquid gallium under pressure, *Sci. Rep.*, 2017, **7**, 5666, DOI: 10.1038/s41598-017-05985-8.

47 E. W. Washburn, The Dynamics of Capillary Flow, *Phys. Rev.*, 1921, **17**, 273, DOI: 10.1103/PhysRev.17.273.

48 F. Delannay, L. Froyen and A. Deruyttere, The wetting of solids by molten metals and its relation to the preparation of metal-matrix composites, *J. Mater. Sci.*, 1987, **22**, 1, DOI: 10.1007/BF01160545.

49 T. Young, An essay on the cohesion of fluids, *Phil. Trans. R. Soc.*, 1805, **95**, 65, DOI: 10.1098/rstl.1805.0005.

50 J. W. Gibbs, On the equilibrium of heterogeneous substances, *Trans. Conn. Acad.*, 1878, **3**, 343, DOI: 10.2475/ajs.s3-16.96.441.

51 M. Strauß, R. Gourgues, M. F. X. Mauser, L. Kulman, M. Castaneda, A. Fognini, A. Shayeghi, P. Geyer and M. Arndt, Superconducting Nanowire Detection of Neutral Atoms and Molecules via Their Internal and Kinetic Energy in the eV Range, *Adv. Phys. Res*, 2025, **4**, 2400133, DOI: 10.1002/apxr.202400133.

52 Y. Ryu, J. Jeong, J. Suh, J. Kim, H. Choi and J. Cha, Utilizing Gate-Controlled Supercurrent for All-Metallic Tunable Superconducting Microwave Resonators, *Nano Lett.*, 2024, **24**(4), 1223, DOI: 10.1021/acs.nanolett.3c04080.

53 Z. Scherübl, M. Kocsis, T. Elalaily, L. Kupás, M. Berke, G. Fülöp, T. Kanne, K. K. Berggren, J. Nygård, S. Csonka and P. Makk, Multimode Operation of a Superconducting Nanowire Switch in the Nanosecond Regime, *ACS Nano*, 2025, **19**(32), 29207, DOI: 10.1021/acsnano.5c03718.

54 M. Horák, V. Čalkovský, J. Mach, V. Křápek and T. Šikola, Plasmonic Properties of Individual Gallium Nanoparticles, *J. Phys. Chem. Lett.*, 2023, **16**, 2012, DOI: 10.1021/acs.jpclett.3c00094.

55 R. R. Sahu, A. S. Ramasamy, S. Bhonsle, M. Vailshery, S. Archana, H. Kumar and T. Das Gupta, Single-step fabrication of liquid gallium nanoparticles via capillary interaction for dynamic structural colours, *Nat. Nanotech.*, 2024, **19**, 766, DOI: **10.1038/s41565-024-01625-1**.

56 Y. Lin, J. Genzer and M. D. Dickey, Attributes, Fabrication, and Applications of Gallium-Based Liquid Metal Particles, *Adv. Sci.*, 2020, **7**, 2000192, DOI: **10.1002/advs.202000192**.

57 W. Lee, R. Ji, U. Gösele and K. Nielsch, Fast fabrication of long-range ordered porous alumina membranes by hard anodization, *Nat. Mater.*, 2006, **5**, 741, DOI: **10.1038/nmat1717**.

58 L. Tomiatti, *Nanoporous Template Analyzer, Zenodo*, 2024, DOI: **10.5281/zenodo.14602027**.

59 B. B. Alchagirov and A. G. Mozgovoi, The Surface Tension of Molten Gallium at HighTemperatures, *High Temp.*, 2005, **43**, 791, DOI: **10.1007/s10740-005-0124-2**.

60 G. F. Strouse, *Standard Reference Material 1751: Gallium Melting-Point Standard*, NIST Special Publication, pp. , pp. 260–157, DOI: **10.6028/NIST.SP.260-157**.

61 V. M. Starov and M. G. Velarde, *Wetting and Spreading Dynamics*, Taylor & FrancisGroup, 2020, 2nd edn, DOI: **10.1201/9780429506246**.

62 M. D. Dickey, R. C. Chiechi, R. J. Larsen, E. A. Weiss, D. A. Weitz and G. M. Whitesides, Eutectic Gallium-Indium (EGaIn): A Liquid Metal Alloy for the Formation of Stable Structures in Microchannels at Room Temperature, *Adv. Funct. Mater.*, 2008, **18**, 1097, DOI: **10.1002/adfm.200701216**.

63 J.-G. Li, Chemical trends in the thermodynamic adhesion of metal/ceramic systems, *Mater. Lett.*, 1995, **22**, 169, DOI: **10.1016/0167-577X(94)00244-4**.

64 H. Zakaria and K. Kenza, Adhesion Phenomenon of Liquid Metals, Liquid Metals, *Intech Open*, 2021, **22**, DOI: **10.5772/intechopen.97419**.

65 P.-G. Gennes, F. B-Wyart and D. Quere, *Capillarity and Wetting Phenomena: Drops, Bubbles, Pearls, Waves*, Springer Science, 2004, DOI: **10.1063/1.1878340**.

66 K. E. Spells, The determination of the viscosity of liquid gallium over an extended range of temperature, *Proc. Phys. Soc.*, 1936, **48**, 299, DOI: **10.1088/0959-5309/48/2/308**.

67 O. K. Rice, The Effect of Pressure on Surface Tension, *J. Chem. Phys.*, 1947, **15**, 333, DOI: **10.1063/1.1746507**.

68 Z. R. Hinton and N. J. Alvarez, Surface tensions at elevated pressure depend strongly on bulk phasesaturation, *J. Coll.Interf. Sci.*, 2021, **594**, 681, DOI: **10.1016/j.jcis.2021.02.114**.

69 P. W. Bridgman, The Effect Of Pressure On The Viscosity Of Forty-Three Pure Liquids, *Proc. Amer. Acad. Arts Sci.*, 1926, **61**, 57, DOI: **10.1016/J.FLUID.2019.06.008**.

70 J. W. P. Schmelzer, E. D. Zanotto and V. M. Fokin, Pressure dependence of viscosity, *J. Chem. Phys.*, 2005, **122**, 074511, DOI: **10.1063/1.1851510**.